Macromolecules

pubs.acs.org/Macromolecules Article

Controlling the Chain Orientation and Crystal Form of Poly(9,9-dioctylfluorene) Films for Low-Threshold Light-Pumped Lasers

Junjie Wang, Yuchao Liu, Deyue Zou, Zhongjie Ren,* Jie Lin,* Xingyuan Liu, and Shouke Yan*

Cite This: *Macromolecules* 2021, 54, 4342–4350 Read Online

ACCESS | Metrics & More | Article Recommendations | Supporting Information

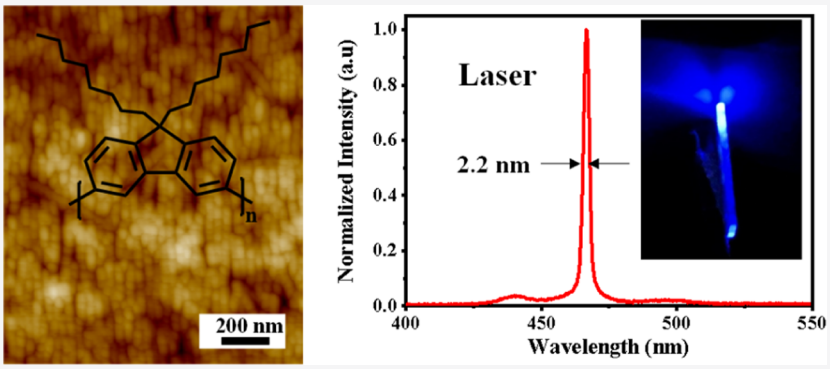

ABSTRACT: Neat thin films of semiconducting polymers are attractive as efficient gain media toward optically pumped lasers. However, the optical loss and out-coupling of isotropic polymer thin films are far from being rationally regulated from the perspective of chain orientation and crystal form. Herein, we accomplished a simultaneous control of both chain orientation and crystal form in large-area highly ordered poly(9,9-dioctylfluorene) (PFO) thin films through epitaxial crystallization. The well-arranged PFO lamellae naturally shape a low-loss, graded-index waveguide to provide spatially distributed optical feedback. Moreover, much more horizontally oriented dipoles significantly enhance the light out-coupling efficiency. Thus, the only 65 nm-thickness oriented PFO films demonstrate excellent amplified spontaneous emission with a low excitation threshold (7.1 $\mu J/cm^2$) and a narrow full width at half-maximum (2.2 nm) measured in the perpendicular direction of PFO chains. This strategy opens an effective pathway to prepare high-performance polymer thin-film lasers and electrically pumped polymer lasers.

INTRODUCTION

The opto-electronic properties of conjugated polymers, which combine the electrical and optical properties of semiconductors with the excellent processing and mechanical properties of plastics, have received widespread interest since 1990.[1,2] They have attracted considerable interest as novel gain media for lasers and optical amplifiers by utilizing their amplified spontaneous emission (ASE) properties.[3−5] Recently, thin-film organic lasers have become a new generation of devices due to their compactness, low cost, mechanical flexibility, as well as being easily pumped from low-power sources.[6,7] Materials chemistry has allowed access to the optically pumped polymeric semiconductor thin-film lasers with a high slope efficiency and a broad lasing wavelength.[8,9] Particularly, neat thin films of semiconducting polymers have been used as efficient gain media toward optically pumped lasers.[10] However, the highly conformational freedom of semiconducting polymers results in complex microstructures of films with randomly arranged and entangled chains, leading to their inferior optical gain to the single crystals of organic small molecules. Hence, structural control of polymeric semiconductors in the condensed state is another vital way for high-performance thin-film lasers. For example, inefficient photon energy transfer to ASE consisting of multiple competing radiative decay pathways can rationally be regulated from the perspective of molecular arrangements.[11] Moreover, horizontally arranged emitting dipoles in polymer layers enable the high optical out-coupling and thus a low-threshold laser.[12,13] However, the regulation mechanism among chain alignments, crystal forms, and ASE or laser properties is far from being well understood.[14] Therefore, it is necessary to adjust the orientation of molecular chains and crystal forms of semiconducting polymers to optimize the laser performance with low optical loss and high gain. These strategies are also important for the realization of electrically pumped polymer lasers. Previous work has established that the close-packed

Received: December 20, 2020
Revised: March 16, 2021
Published: April 21, 2021

https://doi.org/10.1021/acs.macromol.0c02815
Macromolecules 2021, 54, 4342–4350

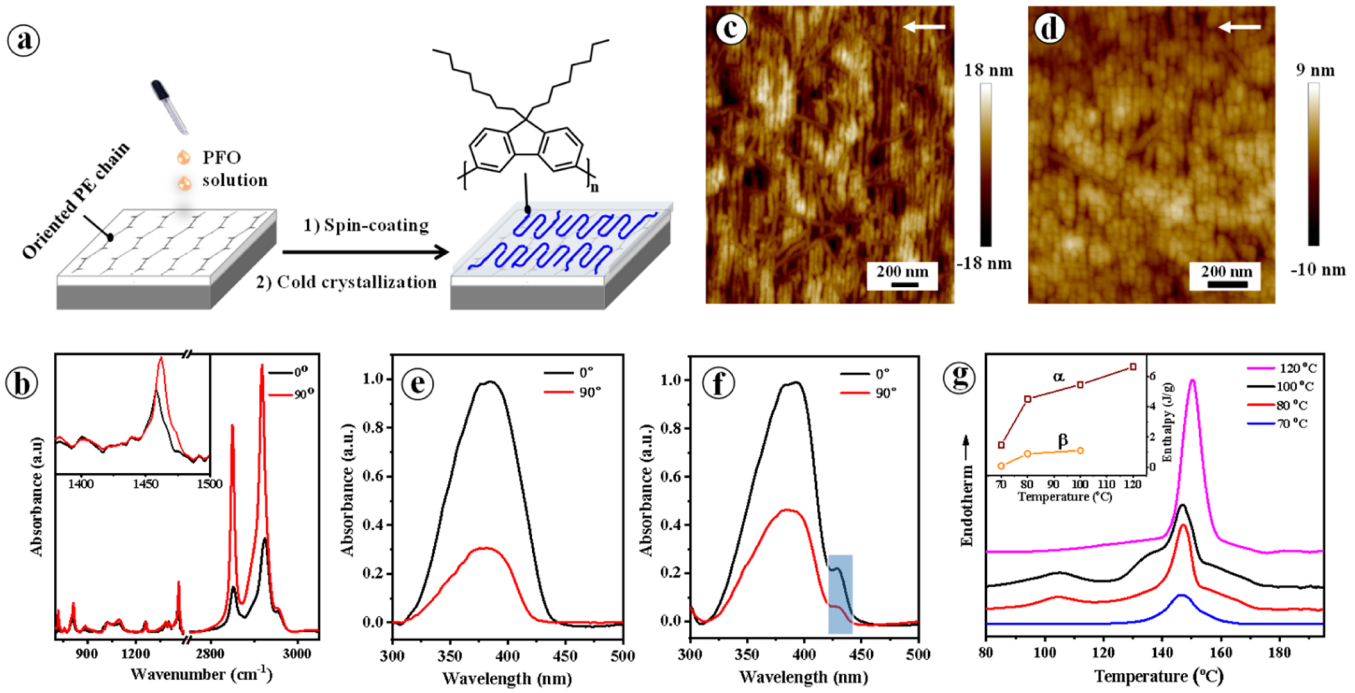

Figure 1. (a) Scheme of the preparation process of PFO crystallized epitaxially on an oriented PE substrate. (b) Polarized FTIR spectra of the PFO-120 thin films. The inset is the enlarged part of characteristic bands in the 1400−1500 cm^{-1} region. The AFM height images of PFO-120 (c) and PFO-100 (d). Polarized UV−vis absorption spectra of PFO-120 (e) and PFO-100 (f). (g) Heating DSC curves of PFO/PE films with cold crystallized at different temperatures. The inset of (g) shows the plots of melting enthalpies of α- and β-PFO crystals against the crystallization temperature. 0 and 90° indicate the electric field vector parallel and perpendicular to the direction of PE molecular chains, respectively. The arrows indicate the direction of PE molecular chains.

arrays of the semiconducting polymer (poly(2-methoxy-5-(2'-ethyl-hexyloxy)-1,4-phenylene vinylene) (MEH-PPV) in the templated nanopore silicas exhibited dramatic improvements in optical gain.[15] The relationship between the chain arrangement, crystal form, and ASE or laser property is, however, not clear because of the lack of modification manipulation. It is thus a challenge to control both the chain orientation and crystal form of large-area well-ordered semiconducting polymer films for lasers. Directional epitaxy has been proved to be efficient for preparing well-ordered thin films of semiconducting polymers with a controlled crystal structure and orientation.[16,17]

Poly(9,9-dioctylfluorene) (PFO) is a prototypical semiconducting polymer with ASE properties, which exhibits large stimulated emission cross sections (10^{-15} cm^2) and high photoluminescence (PL) quantum efficiency.[18,19] PFO is known as a polymorphic material with at least two crystal forms, that is, the α- and β-forms. It is reported that PFO chains in the α and β crystals are packed in the same orthorhombic unit cell with parameters a = 2.56, b = 2.34, and c = 3.32 nm. However, their photophysical properties are totally different based on the intrachain correlation lengths.[20] Moreover, they differ in melting temperature. The melting points of the α- and β-PFO crystals are 157 and 107 °C, respectively.[21] The β-form has attracted great attention due to the effective energy transfer from the amorphous to the β-form and potential for a low-pumped laser.[22,23] Therefore, continuous effort is made to improve the laser properties of randomly oriented spin-coating PFO films.[24]

In this report, large-area highly oriented PFO films are prepared by epitaxy on an oriented polyethylene (PE) substrate. In this way, we accomplish the simultaneous control of both chain orientation and crystal form of the PFO films. The prepared PFO films display dramatic improvements in optical gain without the need for externally imposed optical feedback. Notably, an only 65 nm-thickness-oriented PFO film demonstrates a highly polarized ASE with a low excitation threshold (7.1 $\mu J/cm^2$) and a narrow full width at half maximum (fwhm, 2.2 nm) because the well-arranged lamellae naturally shape a low-loss, graded-index waveguide to provide spatially distributing optical feedback. This strategy opens an effective pathway to prepare high-performance thin-film lasers.

EXPERIMENTAL SECTION

Materials. PFO was purchased from Derthon Optoelectronic Materials Science Technology Co., Ltd. (Shenzhen, China). Its weight-averaged molecular mass (M_w) obtained from GPC (polystyrene standard) is ca. 20 kDa with a polydispersity index of 2.95. High-density PE used in this work was obtained from Lanzhou Petrochemical, China. Its melting point is ca. 135 °C as measured by differential scanning calorimetry (DSC). All of the solvents used in this work were supplied by Beijing Chemical Reagent Co., Ltd. (p.a. grade) and used as received.

Sample Preparation. The preparation of oriented PE films and their typical morphology are presented in Figure S1 of the Supporting Information. PFO/PE double-layered films were prepared by spin-coating (2000 rpm, 60 s) PFO chlorobenzene solution onto the oriented PE substrates at room temperature. The double layers were then routinely dried in vacuum at 40 °C. The epitaxy of PFO on the oriented PE substrate was realized by cold crystallization from the amorphous state at different temperatures below the melting point of PE for 24 h. The related structure characterization and property measurements can be found in the Supporting Information.

ASE Measurements. The pump beam was focused with a cylindrical lens and spatially filtered through an adjustable slit to create a narrow, 200 μm × 5 mm excitation stripe on the films. The

https://doi.org/10.1021/acs.macromol.0c02815
Macromolecules 2021, 54, 4342−4350

fabricated planar waveguides consist of an oriented PFO film (thickness ~65 nm, spin-coating 16 mg/mL PFO chlorobenzene solution) and the oriented PE (thickness ~ 35 nm) together with the polished quartz substrates. To induce stimulated emission, the waveguides were optically pumped at 355 nm with a CryLas GmbH laser, producing 1 ns pulses at a repetition rate of 50 Hz. One end of the stripe was positioned at the substrate edge of the slab waveguide and the edge emission was collected with a fiber-coupled grating spectrograph (Avantes 3048).

RESULTS AND DISCUSSION

Epitaxial Crystallization of PFO on Oriented PE Substrates. As schematically presented in Figure 1a, the epitaxy of PFO was achieved simply by spin-coating its CB solution on the highly oriented PE film and subsequent cold crystallization from the amorphous state at selected temperatures (T_c) for 24 h. The corresponding sample is marked as PFO-T_c. The structures of PFO/PE crystallized at different temperatures were first studied by polarized Fourier transform infrared (FTIR) spectroscopy. Figure 1b shows the polarized FTIR spectra of a PFO-120 thin film. Clearly, the IR bands show obvious anisotropic features.[25] The unique PFO band of the C=C breathing vibration in the aromatic ring at 1460 cm^{-1} exhibits a higher intensity measured with the electric field vector perpendicular to the PE chain direction (90°) than that in the parallel direction (0°), demonstrating the anisotropic alignment of PFO chains. The polarized FTIR spectrum of the PFO-100 thin films (Figure S2) exhibits a close resemblance with Figure 1b, demonstrating an orientation behavior of PFO-100 similar to that of PFO-120. This has been further confirmed by the polarized Raman spectra shown in Figure S3, which exhibit the stronger signal intensity with incident laser polarization parallel (0°) than perpendicular (90°).

It should be noted that the dichroic ratio of PFO-100 is smaller than that of PFO-120. This can be related to (i) a reduced crystallinity since orientation is only achieved in the crystalline due to epitaxial crystallization, (ii) a poor molecular chain orientation, or (iii) even a different spatial arrangement of the PFO molecules, for example, the face-on or edge-on molecular orientations. Therefore, further studies on the orientation structures of PFO crystallized on PE substrates at different temperatures have been conducted by other techniques.

To compare the different crystallization behaviors of PFO on PE substrates and glass slides directly, PFO crystallized in a boundary area between PE and a glass slide was observed by polarized optical microscopy as shown in Figure S4. The boundaries between PE and the glass slide can be clearly seen with the direction of the PE molecular chain parallel to the boundary lines. In the left panel of the optical micrographs, the PE substrates are located in the lower right corners, while the upper left corners present the PFO grown on the neat glass slide. It is evident that PFO on the PE substrate exhibits a much stronger birefringence than that on the glass slide. Considering that the birefringence under a polarized optical microscope is caused by the different double refractive indexes of crystals, a stronger birefringence of the same crystal and orientation structures indicates a higher crystallinity. Since the oriented PE ultrathin films are too thin to show any birefringence,[26,27] a stronger birefringence of PFO grown on PE may demonstrate either a higher crystallinity of PFO grown on PE than on glass or a different crystal structure or/and in-plane crystal orientation. To check the crystallinity of PFO, DSC experiments have been conducted for both PFO-120 and the pure PFO crystallized isothermally on the glass slide also at 120 °C. As presented in Figure S5, while the PFO grown on PE and the glass slide shows the same peak melting temperature at ca. 150 °C, indicating the same crystal modification, a smaller melting enthalpy of pure PFO than PFO-120 (4.95 J/g vs 6.639 J/g) demonstrates indeed a higher crystallinity of PFO crystallized on the PE substrate compared to on the glass slide with the same condition. Moreover, the significant birefringence reduction of PFO/PE double layers after 45° clockwise rotation (right panel of Figure S4) suggests the exceptional anisotropic optical property, that is, the existence of a molecular chain orientation.[26,27] The ordered structure of PFO formed on the PE substrate is revealed by AFM observation. As presented in Figure 1c,d, parallel-aligned slender PFO lamellae arranged perpendicular to the direction of PE chains are clearly seen for both PFO-120 and PFO-100, confirming the epitaxy of PFO on PE substrates. It should be noted that the lamellae formed at 120 °C are, however, somewhat shorter than those formed at 100 °C. Also, the distribution of fwhm obtained from the profiles of AFM phase images analyzed through a build-in PicoView 1.12 software (Figure S6a,b) reveals a thinner lamella of PFO formed at 120 °C than that formed at 100 °C.

The influence of crystallization temperature on the crystallinity of PFO grown on the PE substrate was also studied by DSC experiments. From the DSC curves shown in Figure 1g and the related data listed in Table S1 of the Supporting Information, it is clear that PFO-120 exhibits only one endothermic peak at ca. 150 °C, corresponding to the melting point of α-PFO crystals. On the other hand, PFO-100 exhibits dual melting peaks at 148 and 104 °C, corresponding to the α- and β-PFO crystals, respectively. This demonstrates that partial β-PFO crystals were obtained through crystallization on PE substrates at 100 °C. This can be understood in the following way. The melting temperatures of α- and β-PFO crystals are around 150 and 104 °C, respectively. As a result, crystallization of PFO at 120 °C in its β phase is impossible. At 100 °C, even though the crystallization of PFO in both α and β phases is possible, the crystallization in the β phase should lag behind that in the α phase due to the very small supercooling. In this case, the crystallization of β-PFO could be induced either by the underlying PE or by crystallization in the confined space of early formed α crystals.[28] Since the lack of melting enthalpies of 100% crystalline α- and β-crystals, respectively, we cannot directly get the crystallinity of the α- and β-PFO crystals. However, the absolute melting enthalpy values obtained by DSC can be used to reflect the relative crystallinity of different samples. From the data listed in Table S1, it can be seen that the melting enthalpy of PFO-120 with only α crystals is 6.639 J/g. For PFO-100, the melting enthalpy of α crystals is 5.470 J/g, which is slightly less than that of PFO-120. It exhibits, however, a 1.105 J/g melting enthalpy of β crystals. A total melting enthalpy of 6.675 J/g for PFO-100 may indicate a similar crystallinity with PFO-120. On the other hand, the reduced total melting enthalpy of PFO-80 (4.519 of α + 0.887 of β = 5.406 J/g) demonstrates a crystallinity decrease of PFO crystallized at 80 °C. With a further decrease of the crystallization temperature to 70 °C, an even smaller total melting enthalpy of only 1.545 J/g implies that the crystallization of PFO on the PE substrate is seriously suppressed at 70 °C. The suppressed crystallization of PFO at a low temperature results in the oriented lamellar structure of PFO-80 and PFO-70 unobservable by AFM (Figure S7).

https://doi.org/10.1021/acs.macromol.0c02815
Macromolecules 2021, 54, 4342−4350

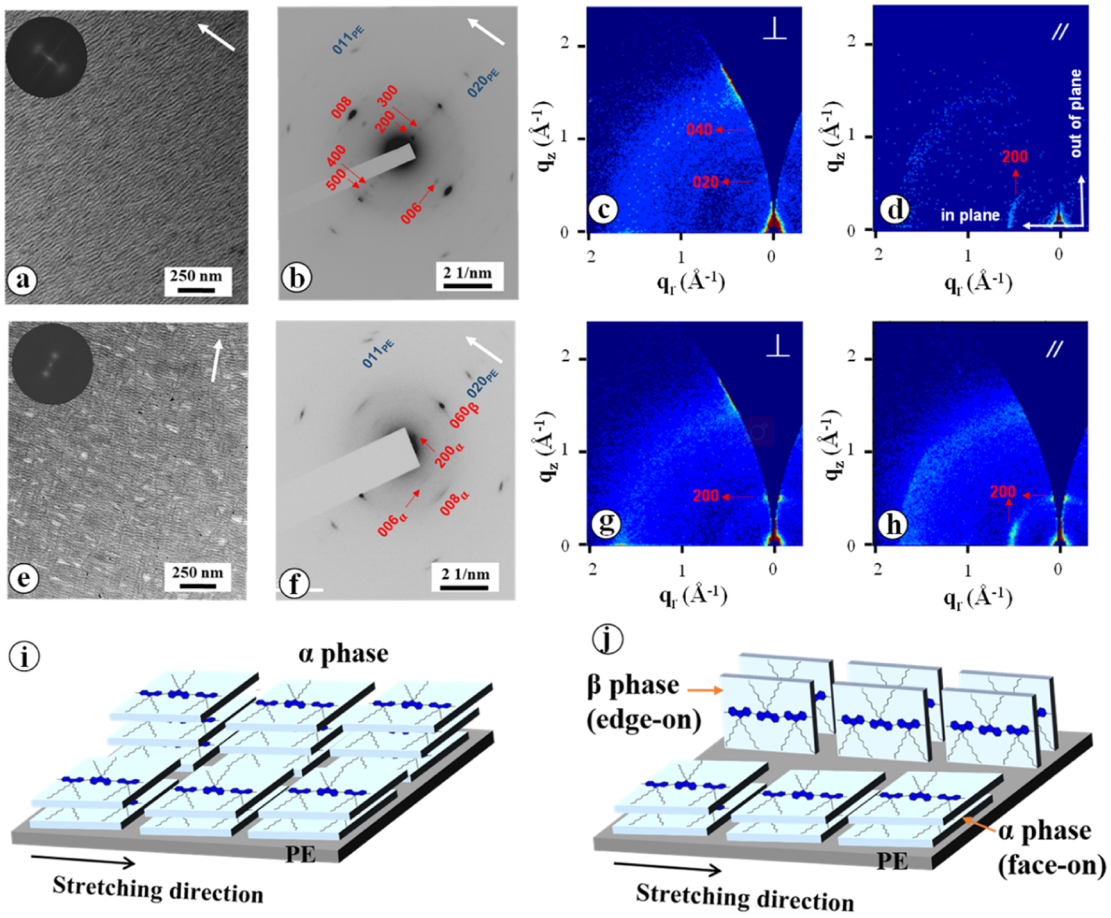

Figure 2. Bright field electron micrographs and corresponding ED patterns of PFO-120 (a,b) and PFO-100 (e,f). 2D-GIXRD maps after the Ewald sphere curvature correction of PFO-120 (c,d) and PFO-100 (g,h) measured with incident X-ray beams perpendicular (⊥) and parallel (||) to the PE chain direction. (i) Molecular stacking of PFO in films obtained at 120 °C with only α crystals. (j) Possible molecular stacking of PFO in films obtained at 100 °C with the α and β mixture. The white arrows indicate the direction of PE molecular chains.

The different structures of PFO grown on PE substrates at different temperatures are also illustrated by the UV−vis experiments. As shown in Figure 1e, PFO-120 shows only a main UV−vis absorption peak at ca. 392 nm, characteristic of α crystals. On the other hand, PFO-100 (Figure 1f) shows a small overlapping shoulder at 430 nm, attributed to β crystals,[20,22] indicating the coexistence of α and β crystals. This is in good agreement with the DSC results. The content of β crystals can be estimated by the area fraction of UV−vis absorption at 430 nm from spectral deconvolution (Figure S8). The contents of β crystals were found to decrease from 4.46% for PFO-100 to 2.81% for PFO-80 and further to 1.08% for PFO-70. Moreover, from the polarized UV−vis absorption spectra (Figures 1e,f and S9), 0 and 90° indicate that the polarization directions of the incident light are parallel and perpendicular to the direction of PE molecular chains, respectively. Typically, the intensity at the direction of light polarization parallel to PE molecular chains (0°) is stronger than that perpendicular to PE molecular chains (90°). The dichroic ratio of UV−vis absorbance is 3.46 for PFO-120 and 2.05 for PFO-100. A further decrease of the dichroic ratio is found for PFO-80 (1.5) and PFO-70 (1.22). According the above-obtained results, it is obvious that the crystallization of PFO on PE substrates at 100 °C is ideal for fabricating well-oriented crystals with the β-PFO content up to 4.46%. Such a high β-form content has never been reported before, which is thus a potential material for a pumped laser.

The detailed orientation structure and mutual relationship between PFO and PE were further studied by transmission electron microscopy (TEM) combined with electron diffraction (ED) as well as the 2D-grazing incidence X-ray diffraction (GIXRD) technique.[29,30] Similarly oriented lamellar structures were observed in phase contrast bright field electron micrographs (Figure 2a,e). The fast Fourier transform of the bright field image inserted in Figure 2a,e demonstrates a lamellar periodicity of ca. 25 nm for PFO-120 and 29 nm for PFO-100, respectively. The appearance of well-defined reflection spots of PE and PFO in the ED patterns (Figures 2b,f and S10) indicates the high orientation of both polymers. All of the diffractions can be accounted for by the orthorhombic unit cells of either PFO or PE.[20,31] The alignment of weak (006) and clear (008) diffraction spots of PFO along (002) reflection spots of PE indicates again a parallel chain orientation of both polymers. With close inspection, the ED pattern of PFO-120 (Figure 2b) is somewhat different from that of PFO-100 (Figure 2f). For PFO-120, the appearance of a series of (h00) diffraction spots indicates an in-plane arrangement of the a-axis, that is, a b-axis orientation, which has been further confirmed by 2D-GIXRD experiments, see the 2D-GIXRD patterns corrected for the Ewald sphere in Figure 2c,d, as well as the corresponding

https://doi.org/10.1021/acs.macromol.0c02815
Macromolecules 2021, 54, 4342−4350

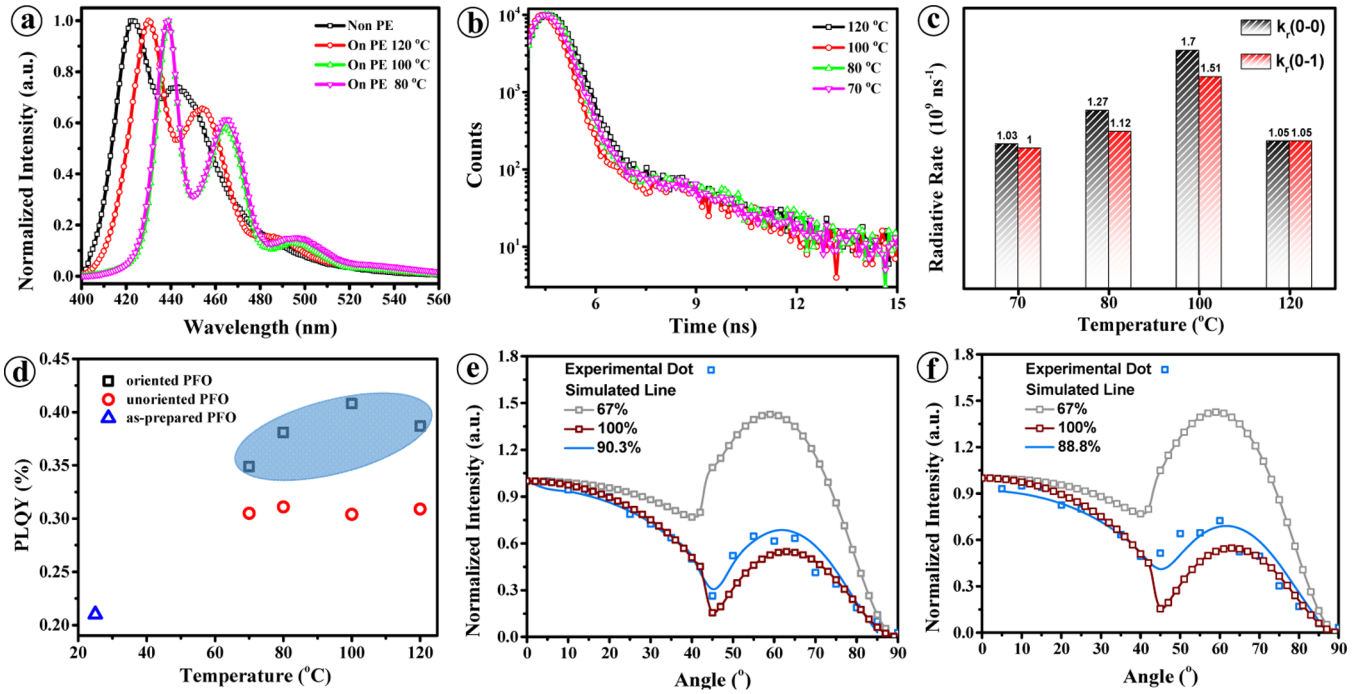

Figure 3. (a) PL spectra of PFO thin films with different processing conditions. (b) Fluorescence radiative rates of the oriented PFO films for the 0−1 band emission with different crystallization temperatures. (c) Fluorescence radiative rates at 0−0 and 0−1 vibronic bands of the oriented PFO films with different crystallization temperatures. (d) PLQY of PFO thin films with different processing conditions. The angle- and polarization-resolved PL of PFO-120 (e) and PFO-100 (f).

originally obtained patterns in Figure S11. Accordingly, the crystal stacking of face-on oriented PFO molecules in its α-form is illustrated in Figure 2i.

In the ED pattern of PFO-100, except for (200), very weak (060) diffraction arcs can be identified with close inspection (Figure 2f), which is overlapped with the strong (110) diffraction of PE. The coexistence of (200) and (060) was also confirmed by the 2D-GIXRD experiments.

The 2D-GIXRD of PFO-100 measured with the incidence X-ray parallel to the PE chain direction shown in Figure 2h looks very different from that shown in Figure 2d, especially in the high-q range close to the expected reflections of PE. This is caused by the change of orientation status of PE films annealed at different temperatures.[32] As seen from the ED patterns in Figure S10, the (002) diffraction arcs of PE in PFO-120 are evidently narrower than those in PFO-100. This indicates the higher *c*-axis orientation of PFO-120 than of PFO-100, reflecting a smaller inclination angle of the *c*-axis with respect to the drawing direction. This does not influence the out-of-plane 2D-GIXRD pattern measured vertically to the *c*-axis owing to the random rotation of *a*- and *b*-axes about the *c*-axis. It exhibits, however, a great influence on the out-of-plane 2D-GIXRD pattern when measured along the chain direction. Taking the 0.2° incidence angle used for the X-ray measurement into account, if the chain, namely, the *c*-axis, is perfectly and strictly along the drawing direction, there will be no (*hk*0) diffractions of PE at all. Moreover, the $(200)_{PFO}$ spot shows up in both the in-plane and out-of-plane directions when measured with the incidence X-ray parallel to the direction of PE chains. One may attribute this to a fiber orientation of PFO with the *c*-axis aligned in the PE chains' direction and a random rotation of *a*- and *b*-axes around the *c*-axis. If this is true, the intense PFO reflections of (330), (140), and (420) should then be observed.[33] This is, however, not the case. These experimental results suggest the formation of two populations of oriented PFO crystals on oriented PE at 100 °C. They have the unique chain orientation in the film plane along the direction of the PE chains, while their *a*-axis and *b*-axis are arranged in the film normal direction, respectively. Combining the facts that α-PFO crystals formed at 120 °C exhibit only a *b*-axis orientation and the coexistence of α and β crystals in films formed at 100 °C, one may simply correlate the PFO crystals with an *a*-axis orientation to its β counterparts, which coexist with the predominant *b*-axis-oriented α crystals as illustrated schematically in Figure 2j. This can, however, not be confirmed at moment and will be studied further through other suitable techniques. Here in this work, we pay attention mainly to the influence of the crystal and orientation structures on the performance of the related PFO thin films.

Photophysical Properties and ASE. PL spectra of PFO thin films with different processing conditions were determined. The pure PFO without the PE substrate shows the characteristic emissions at 422 and 443 nm (Figure 3a). They are assigned to the 0−0 band of the amorphous phase and the 0−1 band of the mixed amorphous and α-form, respectively. For PFO-120, the amorphous phase emission at 422 nm disappears, reflecting a high crystallinity of PFO. Meanwhile, it displays the characteristic emission of α-form crystals at 430 nm (0−0 band), 455 nm (0−1 band), and 487 nm (0−2 band). For PFO-100, the well-resolved red-shifted vibronic transitions at 439 nm (0−0 band), 466 nm (0−1 band), and 497 nm (0−2 band) can be observed, which is the typical emission of the PFO containing some extent of β crystals and well consistent with the previous reports.[19,33−35] The similar emission behavior of PFO-80 is observed with PFO-100, even though its β crystal content is much lower than that of PFO-100.

https://doi.org/10.1021/acs.macromol.0c02815
Macromolecules 2021, 54, 4342−4350

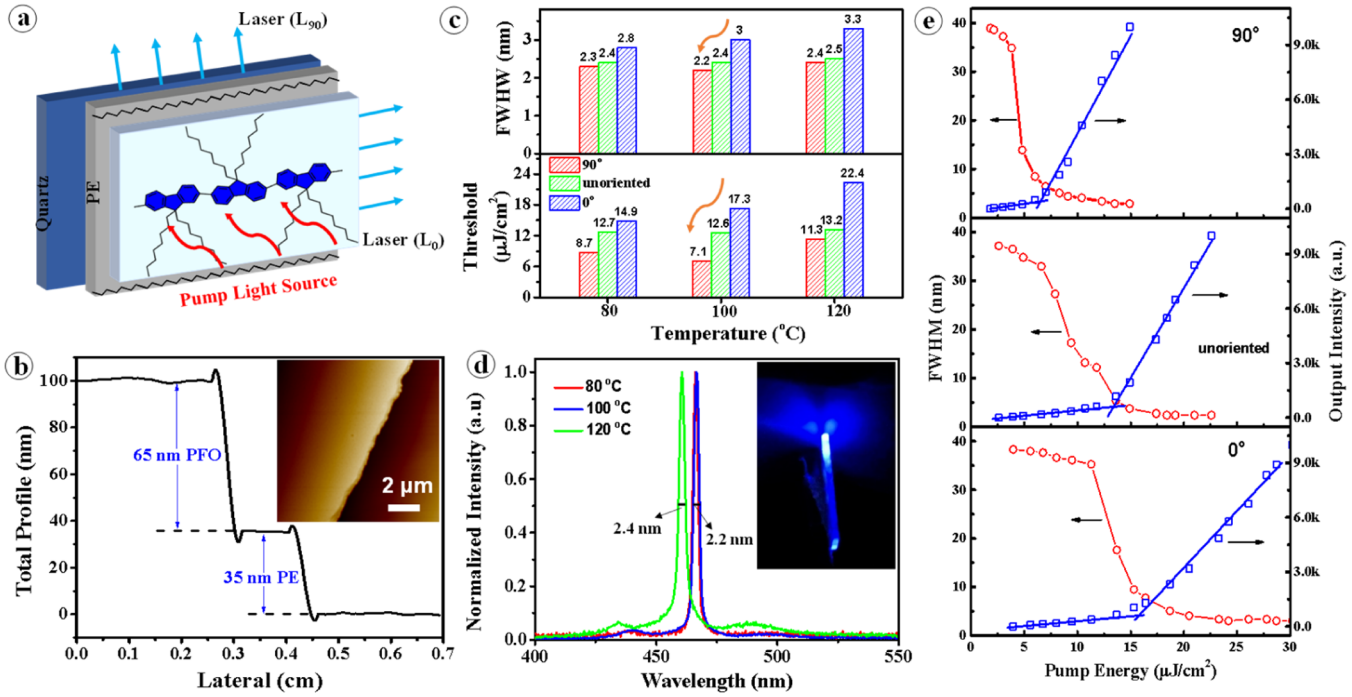

Figure 4. (a) Schematic illustration for ASE lasers of the oriented PFO/PE films excited by a pump light source measured in different directions. (b) Film thickness of PFO for ASE measurements determined by Profiler. The inset is an AFM height image at the interface of PFO and PE. (c) Excitation thresholds and fwhm's of the oriented PFO/PE films crystallized at different temperatures and measured in different directions. (d) Normalized ASE spectra collected from the edge of PFO/PE films above the threshold pump energy. (e) Pump energy-dependent profiles of output intensities and fwhm's measured in different directions for PFO-100.

The PL decay of PFO can be fitted as double exponential values by time-resolved PL measurements (Figures 3b and S12). The apparent decay times change slightly with the crystallization temperatures (Figure 3c and Table S2). The films of PFO-100 decay in a very fast way with short lifetimes and high radiative rates (1.7×10^9 ns^{-1} for 0−0 band and 1.51×10^9 ns^{-1} for 0−1 band), which may be related to the differently oriented structure and high content of the β crystals (Figure 3c and Table S3). Emitting dipole orientations of PFO films were characterized by angle- and polarization-resolved PL.[36,37] The determined curves are compared to fitted curves with different horizontal dipole ratios $\Theta_{\parallel}$ (e.g., $\Theta_{\parallel}$ = 100% for fully horizontal dipoles and $\Theta_{\parallel}$ = 67% for the isotropic dipole orientation) to extract $\Theta_{\parallel}$, which is thus measured to be 90.3% for PFO-120 (Figure 3e). The results indicate that PFO films have more horizontally oriented dipoles than vertically oriented ones and thus high light out-coupling efficiency can be expected. Similarly, PFO-100 films also show the high $\Theta_{\parallel}$ with 88.8% (Figure 3f). The oriented microstructures with high light out-coupling efficiency endow PFO films high PL quantum efficiency (PLQY). With the same thickness, the unoriented PFO films crystallized at a high temperature display the obviously higher PLQY than the non-crystallized ones (Figure 3d). Furthermore, the oriented PFO films show the highest PLQY due to the enhanced horizontally oriented dipoles. It is noted that the oriented PFO-100 films manifest a higher PLQY of 40.8% than 38.7% of the PFO-120 films, attributed to the existence of β crystals.[38]

For ASE property characterization, the output lights parallel (L_0) and perpendicular (L_{90}) to the direction of PFO chains were detected (Figure 4a). In our case, the planar waveguides have been fabricated by 65 nm-thickness PFO films and 35 nm-thickness PE films together with a quartz substrate (Figure 4b). It is noteworthy that the thickness of PFO is much thinner than that used in previous reports (100−300 nm).[39,40] After applying enough pump energy, all PFO films crystallized at different temperatures show the narrowing of PL spectra at 0−1 bands, accompanied by the dramatic increase of the peak and overall emission intensity, reflecting the presence of ASE (Figures S13−S15).[41] Similar to PL spectra, the ASE peak of PFO-120 (460 nm) displays an obvious blue shift compared with those of PFO-80 and PFO-100 (466 nm) (Figure 4d). Additionally, the oriented PFO films show a waveguide laser pattern with a double-lobed profile after spectral narrowing, arising from an anti-symmetric near-field phase (inset of Figure 4d).[42,43] We can clearly see from Figure 4e that the different light output directions exhibit substantially various ASE thresholds for PFO-100, which can also be observed for other films crystallized at different temperatures (Figures S16 and S17). Moreover, regardless of crystallization temperatures, the threshold measured with the output light perpendicular to PFO chains (L_{90}) is always lower than in the parallel direction (L_0) (Table S4). The low threshold at L_{90} is due to more horizontally oriented dipoles than vertically oriented ones and thus a high light out-coupling efficiency (Figure 2i,j). As a matter of fact, a minimum threshold of 7.1 $\mu J/cm^2$ (L_{90}) is obtained for PFO-100 films. The threshold of the unoriented counterpart is 12.6 $\mu J/cm^2$, 1.78 times higher than L_{90}. The thresholds of L_{90} for PFO-80 and PFO-100 are relatively smaller than for PFO-120, which may be caused by the existing β-form crystals (Figure 4c). Furthermore, the low threshold of L_{90} for PFO-100 is attributed to the high extent of orientation and high k_r compared with that of PFO-80. As mentioned above, the highest k_r at the 0−1 band for PFO-100 films accounts for the lowest ASE threshold since the radiative decay rate is directly related to Einstein's B coefficient as expressed

https://doi.org/10.1021/acs.macromol.0c02815
Macromolecules 2021, 54, 4342−4350

by the equation $B \sim (c/8\pi h\nu_0^3)k_r$, which is inversely proportional to the ASE threshold.[44] fwhm is another important parameter of ASE performance, which affects the purity of the excited laser. It is clear that the fwhm of L_{90} for PFO-100 is only 2.208 nm, which is much lower than that of L_0 (3.045 nm) and the unoriented films (2.4 nm). There is excellent ASE performance of the oriented PFO film with only 65 nm-thickness, a low threshold of 7.1 μJ/cm^2, and a narrow fwhm of only 2.208 nm. As far as we know, in the reported references, it is the thinnest polymeric film displaying ASE lasers with a low threshold and a narrow fwhm.[19,45−47] The improved ASE performance is not only attributed to the high orientation of molecular chains and β-form crystals in PFO films, but also the periodically arranged lamellae that acted as a spatially optical distributed feedback (DFB) structure are also conducive to laser conduction and out-coupling.[48] It is noted that the DFB structure can be easily and naturally formed during epitaxial crystallization instead of etching and other complex methods,[49,50] which greatly simplify the preparation technology and lower the cost. The stability of ASE performance is also detected under 8 μJ/cm^2 pulse in ambient air at room temperature and the ASE intensity is nearly unchanged within 65 min for PFO-100. It should be emphasized that the oriented PFO films are neither encapsulated nor in an N_2 atmosphere, suggesting their potential for gain media in laser applications.

CONCLUSIONS

In summary, oriented PFO films with the parallelly aligned lamellar structures were successfully prepared via epitaxial crystallization on highly oriented PE substrates. The crystal structures and arrangements of PFO molecules in the films can be simply tuned by the crystallization temperatures. Pure α-form crystals with a maximum dichroic ratio measured by UV−vis absorbance of 3.46 have been obtained at a crystallization temperature of 120 °C. On the other hand, coexistence of α and β crystals can be achieved at lower crystallization temperatures, for example, 100 and 80 °C. The TEM and 2D-GIXRD results demonstrate a face-on orientation of the PFO molecular chains in the films with only α crystals, while a mixture of face-on and edge-on oriented PFO molecular chains are observed in the films containing both α and β crystals. It has been confirmed that the different crystal and orientation structures influence the performance of the PFO films remarkably. PL decay measurements reveal that the oriented PFO-100 films containing both α and β crystals and a high ratio of β crystals decay in a much faster way with a short lifetime and a high radiative rate. For ASE properties, the oriented PFO films with well-arranged lamellae shape the DFB laser structure naturally. With the synergetic effect of the horizontally oriented dipoles and DFB structure, we can obtain ASE with a very low threshold (7.1 μJ/cm^2) and a narrow fwhm (2.2 nm) in only 65 nm-thick films. In addition, the stability of the ASE laser is excellent and the ASE intensity does not decline within 65 min. It is clear that epitaxial crystallization provides a simple and efficient way to produce large-area, highly oriented PFO films for low-threshold thin-film lasers.

ASSOCIATED CONTENT

Supporting Information

The Supporting Information is available free of charge at https://pubs.acs.org/doi/10.1021/acs.macromol.0c02815.

Structure characterization and property measurements; AFM images and an ED pattern of the PE oriented thin films; polarized FTIR spectrum of PFO-100; polarized Raman spectra of PFO-120 and PFO-100; polarized light microscopy micrographs of PFO-120 and PFO-100; the DSC curves of PFO-120 and pure PFO crystallized isothermally at 120 °C; AFM phase images of PFO-120 and PFO-100; AFM height and phase images of PFO-80 and PFO-70; deconvolution of the UV−vis absorption spectra for PFO-120, PFO-100, PFO-80, and PFO-70; polarized UV−vis absorption spectra of PFO-80 and PFO-70; the ED patterns of PFO-120 and PFO-100; 2D-GIXRD maps of PFO-120 and PFO-100; fluorescence decay times at 0−0, 0−1, and 0−2 vibronic bands; evolution of emission spectra under pulsed excitation at different powers with the different measured directions for PFO-80, PFO-100, and PFO-120; pump energy-dependent profiles of output intensities and fwhm for PFO-80 and PFO-100; and polarized UV−vis absorbance spectra of oriented PFO films spin-coated from chloroform solution (PDF)

AUTHOR INFORMATION

Corresponding Authors

Zhongjie Ren − *State Key Laboratory of Chemical Resource Engineering, College of Materials Science and Engineering, Beijing University of Chemical Technology, Beijing 100029, China;* orcid.org/0000-0002-7981-4431; Email: renzj@mail.buct.edu.cn

Jie Lin − *State Key Laboratory of Luminescence and Applications, Changchun Institute of Optics, Fine Mechanics and Physics, Chinese Academy of Science, Changchun 130033, P. R. China;* orcid.org/0000-0001-9676-2218; Email: linj@ciomp.ac.cn

Shouke Yan − *State Key Laboratory of Chemical Resource Engineering, College of Materials Science and Engineering, Beijing University of Chemical Technology, Beijing 100029, China; Key Laboratory of Rubber-Plastics, Ministry of Education, Qingdao University of Science & Technology, Qingdao 266042, P. R. China;* orcid.org/0000-0003-1627-341X; Email: skyan@mail.buct.edu.cn

Authors

Junjie Wang − *State Key Laboratory of Chemical Resource Engineering, College of Materials Science and Engineering, Beijing University of Chemical Technology, Beijing 100029, China*

Yuchao Liu − *State Key Laboratory of Chemical Resource Engineering, College of Materials Science and Engineering, Beijing University of Chemical Technology, Beijing 100029, China; Key Laboratory of Rubber-Plastics, Ministry of Education, Qingdao University of Science & Technology, Qingdao 266042, P. R. China*

Deyue Zou − *State Key Laboratory of Luminescence and Applications, Changchun Institute of Optics, Fine Mechanics and Physics, Chinese Academy of Science, Changchun 130033, P. R. China*

Xingyuan Liu − *State Key Laboratory of Luminescence and Applications, Changchun Institute of Optics, Fine Mechanics and Physics, Chinese Academy of Science, Changchun 130033, P. R. China;* orcid.org/0000-0002-9681-1646

Complete contact information is available at:

https://pubs.acs.org/10.1021/acs.macromol.0c02815

Notes

The authors declare no competing financial interest.

■ ACKNOWLEDGMENTS

The authors thank Prof. Dr. J. Zhang for the helpful discussion on structure analysis. The financial support of the National Natural Science Foundation of China (nos. 51922021 and 52027804) and Shandong Provincial Natural Science Foundation (ZR2019ZD50) is gratefully acknowledged.

■ REFERENCES

(1) Liu, Y.; Li, C.; Ren, Z.; Yan, S.; Bryce, M. R. All-organic thermally activated delayed fluorescence materials for OLEDs. *Nat. Rev. Mater.* **2018**, *3*, 18020.

(2) Peet, J.; Kim, J. Y.; Coates, N. E.; Ma, W. L.; Moses, D.; Heeger, A. J.; Bazan, G. C. Efficiency enhancement in low-bandgap polymer solar cells by processing with alkane dithiols. *Nat. Mater.* **2007**, *6*, 497−500.

(3) Hsu, Y.-T.; Tai, C.-T.; Wu, H.-M.; Hou, C.-F.; Liao, Y.-M.; Liao, W.-C.; Haider, G.; Hsiao, Y.-C.; Lee, C.-W.; Chang, S.-W.; Chen, Y.-H.; Wu, M.-H.; Chou, R.-J.; Bera, K. P.; Lin, Y.-Y.; Chen, Y.-Z.; Kataria, M.; Lin, S.-Y.; Paul Inbaraj, C. R.; Lin, W.-J.; Lee, W.-Y.; Lin, T.-Y.; Lai, Y.-C.; Chen, Y.-F. Self-Healing Nanophotonics: Robust and Soft Random Lasers. *ACS Nano* **2019**, *13*, 8977−8985.

(4) Gather, M. C.; Meerholz, K.; Danz, N.; Leosson, K. Net optical gain in a plasmonic waveguide embedded in a fluorescent polymer. *Nat. Photonics* **2010**, *4*, 457−461.

(5) Mikosch, A.; Ciftci, S.; Kuehne, A. J. C. Colloidal crystal lasers from monodisperse conjugated polymer particles via bottom-up coassembly in a sol-gel matrix. *ACS Nano* **2016**, *10*, 10195−10201.

(6) Clark, J.; Lanzani, G. Organic photonics for communications. *Nat. Photonics* **2010**, *4*, 438−446.

(7) Samuel, I. D. W.; Turnbull, G. A. Organic semiconductor lasers. *Chem. Rev.* **2007**, *107*, 1272−1295.

(8) Xia, R.; Lai, W.-Y.; Levermore, P. A.; Huang, W.; Bradley, D. D. C. Low-threshold distributed-feedback lasers based on pyrene-cored starburst molecules with 1,3,6,8-attached oligo(9,9-dialkylfluorene) arms. *Adv. Funct. Mater.* **2009**, *19*, 2844−2850.

(9) Tsiminis, G.; Wang, Y.; Kanibolotsky, A. L.; Inigo, A. R.; Skabara, P. J.; Samuel, I. D. W.; Turnbull, G. A. Nanoimprinted organic semiconductor laser pumped by a light-emitting diode. *Adv. Mater.* **2013**, *25*, 2826−2830.

(10) Yap, B. K.; Xia, R.; Campoy-Quiles, M.; Stavrinou, P. N.; Bradley, D. D. C. Simultaneous optimization of charge-carrier mobility and optical gain in semiconducting polymer films. *Nat. Mater.* **2008**, *7*, 376−380.

(11) Bolla, G.; Liao, Q.; Amirjalayer, S.; Tu, Z.; Lv, S.; Liu, J.; Zhang, S.; Zhen, Y.; Yi, Y.; Liu, X.; Fu, H.; Fuchs, H.; Dong, H.; Wang, Z.; Hu, W. Cocrystallization tailoring multiple radiative decay pathways for amplified spontaneous emission. *Angew. Chem., Int. Ed.* **2021**, *60*, 285−293.

(12) Zeng, W.; Lai, H.-Y.; Lee, W.-K.; Jiao, M.; Shiu, Y.-J.; Zhong, C.; Gong, S.; Zhou, T.; Xie, G.; Sarma, M.; Wong, K.-T.; Wu, C.-C.; Yang, C. Achieving nearly 30% external quantum efficiency for orange-red organic light emitting diodes by employing thermally activated delayed fluorescence emitters composed of 1,8-naphthalimide-acridine hybrids. *Adv. Mater.* **2018**, *30*, 1704961.

(13) Kim, S.-Y.; Jeong, W.-I.; Mayr, C.; Park, Y.-S.; Kim, K.-H.; Lee, J.-H.; Moon, C.-K.; Brütting, W.; Kim, J.-J. Organic light-emitting diodes with 30% external quantum efficiency based on a horizontally oriented emitter. *Adv. Funct. Mater.* **2013**, *23*, 3896−3900.

(14) Kuehne, A. J. C.; Gather, M. C. Organic lasers: recent developments on materials, device geometries, and fabrication techniques. *Chem. Rev.* **2016**, *116*, 12823−12864.

(15) Martini, I. B.; Craig, I. M.; Molenkamp, W. C.; Miyata, H.; Tolbert, S. H.; Schwartz, B. J. Controlling optical gain in semiconducting polymers with nanoscale chain positioning and alignment. *Nat. Nanotechnol.* **2007**, *2*, 647−652.

(16) Trefz, D.; Gross, Y. M.; Dingler, C.; Tkachov, R.; Hamidi-Sakr, A.; Kiriy, A.; McNeill, C. R.; Brinkmann, M.; Ludwigs, S. Tuning orientational order of highly aggregating P(NDI2OD-T2) by solvent vapor annealing and blade coating. *Macromolecules* **2019**, *52*, 43−54.

(17) Jiang, S.; Qian, H.; Liu, W.; Wang, C.; Wang, Z.; Yan, S.; Zhu, D. Vapor phase epitaxy of perylo[1,12-b,c,d]thiophene on highly oriented polyethylene thin films. *Macromolecules* **2009**, *42*, 9321−9324.

(18) O'Carroll, D.; Lieberwirth, I.; Redmond, G. Microcavity effects and optically pumped lasing in single conjugated polymer nanowires. *Nat. Nanotechnol.* **2007**, *2*, 180−184.

(19) Rothe, C.; Galbrecht, F.; Scherf, U.; Monkman, A. The *β*-Phase of Poly(9,9-dioctylfluorene) as a Potential System for Electrically Pumped Organic Lasing. *Adv. Mater.* **2006**, *18*, 2137−2140.

(20) Grell, M.; Bradley, D. D. C.; Ungar, G.; Hill, J.; Whitehead, K. S. Interplay of physical structure and photophysics for a liquid crystalline polyfluorene. *Macromolecules* **1999**, *32*, 5810−5817.

(21) Chen, S. H.; Su, A. C.; Chen, S. A. Noncrystalline Phases in Poly(9,9-di-n-octyl-2,7-fluorene). *J. Phys. Chem. B* **2005**, *109*, 10067−10072.

(22) Lu, H.-H.; Liu, C.-Y.; Chang, C.-H.; Chen, S.-A. Self-dopant formation in poly(9,9-di-n-octylfluorene) via a dipping method for efficient and stable pure-blue electroluminescence. *Adv. Mater.* **2007**, *19*, 2574−2579.

(23) Becker, K.; Lupton, J. M. Dual species emission from single polyfluorene molecules: signatures of stress-induced planarization of single polymer chains. *J. Am. Chem. Soc.* **2005**, *127*, 7306−7307.

(24) Yi, J.; Niu, Q.; Xu, W.; Hao, L.; Yang, L.; Chi, L.; Fang, Y.; Huang, J.; Xia, R. Significant lowering optical loss of electrodes via using conjugated polyelectrolytes interlayer for organic laser in electrically driven device configuration. *Sci. Rep.* **2016**, *6*, 25810.

(25) Caricato, A. P.; Anni, M.; Manera, M. G.; Martino, M.; Rella, R.; Romano, F.; Tunno, T.; Valerini, D. Study of temperature dependence and angular distribution of poly(9,9-dioctylfluorene) polymer films deposited by matrix-assisted pulsed laser evaporation (MAPLE). *Appl. Surf. Sci.* **2009**, *255*, 9659−9664.

(26) Hu, J.; Xin, R.; Hou, C.-Y.; Yan, S.-K.; Liu, J.-C. Direct Comparison of Crystal Nucleation Activity of PCL on Patterned Substrates. *Chin. J. Polym. Sci.* **2019**, *37*, 693−699.

(27) Zhou, H.; Jiang, S.; Yan, S. Epitaxial crystallization of poly(3-hexylthiophene) on a highly oriented polyethylene thin film from solution. *J. Phys. Chem. B* **2011**, *115*, 13449−13454.

(28) De Rosa, C.; Di Girolamo, R.; Auriemma, F.; D'Avino, M.; Talarico, G.; Cioce, C.; Scoti, M.; Coates, G. W.; Lotz, B. Oriented microstructures of crystalline-crystalline block copolymers induced by epitaxy and competitive and confined crystallization. *Macromolecules* **2016**, *49*, 5576−5586.

(29) Factor, B. J.; Russell, T. P.; Toney, M. F. Grazing incidence X-ray scattering studies of thin films of an aromatic polyimide. *Macromolecules* **1993**, *26*, 2847−2859.

(30) Balko, J.; Portale, G.; Lohwasser, R. H.; Thelakkat, M.; Thurn-Albrecht, T. Surface induced orientation and vertically layered morphology in thin films of poly(3-hexylthiophene) crystallized from the melt. *J. Mater. Res.* **2017**, *32*, 1957−1968.

(31) Minke, R.; Blackwell, J. Single crystals of poly(tetramethylene Adipate). *J. Macromol. Sci., Part B: Phys.* **1980**, *18*, 233−255.

(32) Li, J.; Xue, M.; Xue, N.; Li, H.; Zhang, L.; Ren, Z.; Yan, S.; Sun, X. Highly Anisotropic P3HT Film Fabricated via Epitaxy on an Oriented Polyethylene Film and Solvent Vapor Treatment. *Langmuir* **2019**, *35*, 7841−7847.

(33) Chen, S. H.; Su, A. C.; Su, C. H.; Chen, S. A. Crystalline forms and emission behavior of poly(9,9-di-n-octyl-2,7-fluorene). *Macromolecules* **2005**, *38*, 379−385.

(34) Ariu, M.; Sims, M.; Rahn, M. D.; Hill, J.; Fox, A. M.; Lidzey, D. G.; Oda, M.; Cabanillas-Gonzalez, J.; Bradley, D. D. C. Exciton migration in *β*-phase poly(9,9-dioctylfluorene). *Phys. Rev. B: Condens. Matter Mater. Phys.* **2003**, *67*, 195333.

(35) Hung, M.-C.; Liao, J.-L.; Chen, S.-A.; Chen, S.-H.; Su, A.-C. Fine tuning the purity of blue emission from polydioctylfluorene by end-capping with electron-deficient moieties. *J. Am. Chem. Soc.* **2005**, *127*, 14576−14577.
(36) Lin, T.-A.; Chatterjee, T.; Tsai, W.-L.; Lee, W.-K.; Wu, M.-J.; Jiao, M.; Pan, K.-C.; Yi, C.-L.; Chung, C.-L.; Wong, K.-T.; Wu, C.-C. Sky-blue organic light emitting diode with 37% external quantum efficiency using thermally activated delayed fluorescence from spiroacridine-triazine hybrid. *Adv. Mater.* **2016**, *28*, 6976−6983.
(37) Kaji, H.; Suzuki, H.; Fukushima, T.; Shizu, K.; Suzuki, K.; Kubo, S.; Komino, T.; Oiwa, H.; Suzuki, F.; Wakamiya, A.; Murata, Y.; Adachi, C. Purely organic electroluminescent material realizing 100% conversion from electricity to light. *Nat. Commun.* **2015**, *6*, 8476.
(38) Endo, T.; Kobayashi, T.; Nagase, T.; Naito, H. Anisotropic optical properties of aligned β-phase polyfluorene thin films. *Thin Solid Films* **2008**, *517*, 1324−1326.
(39) Ryu, G.; Xia, R.; Bradley, D. D. C. Optical gain characteristics of β-phase poly(9,9-dioctylfluorene). *J. Phys.: Condens. Matter* **2007**, *19*, 056205.
(40) Calzado, E. M.; Villalvilla, J. M.; Boj, P. G.; Quintana, J. A.; Díaz-García, M. A. Tuneability of amplified spontaneous emission through control of the thickness in organic-based waveguides. *J. Appl. Phys.* **2005**, *97*, 093103.
(41) Xia, H.; Hu, C.; Chen, T.; Hu, D.; Zhang, M.; Xie, K. Advances in conjugated polymer lasers. *Polymers* **2019**, *11*, 443.
(42) Qin, C.; Sandanayaka, A. S. D.; Zhao, C.; Matsushima, T.; Zhang, D.; Fujihara, T.; Adachi, C. Stable room-temperature continuous-wave lasing in quasi-2D perovskite films. *Nature* **2020**, *585*, 53−57.
(43) Shukla, A.; Wallwork, N. R.; Li, X.; Sobus, J.; Mai, V. T. N.; McGregor, S. K. M.; Chen, K.; Lepage, R. J.; Krenske, E. H.; Moore, E. G.; Namdas, E. B.; Lo, S. C. Deep-Red Lasing and Amplified Spontaneous Emission from Nature Inspired Bay-Annulated Indigo Derivatives. *Adv. Opt. Mater.* **2020**, *8*, 1901350.
(44) Kim, D.-H.; Sandanayaka, A. S. D.; Zhao, L.; Pitrat, D.; Mulatier, J. C.; Matsushima, T.; Andraud, C.; Ribierre, J. C.; Adachi, C. Extremely low amplified spontaneous emission threshold and blue electroluminescence from a spin-coated octafluorene neat film. *Appl. Phys. Lett.* **2017**, *110*, 023303.
(45) Heliotis, G.; Xia, R.; Bradley, D. D. C.; Turnbull, G. A.; Samuel, I. D. W.; Andrew, P.; Barnes, W. L. Blue, surface-emitting, distributed feedback polyfluorene lasers. *Appl. Phys. Lett.* **2003**, *83*, 2118−2120.
(46) Zhang, D.; Chen, Z.; Ma, D. White light emission on amplified spontaneous emission with dye content controlled polymer system. *J. Appl. Phys.* **2008**, *103*, 123103.
(47) Heliotis, G.; Xia, R.; Whitehead, K. S.; Turnbull, G. A.; Samuel, I. D. W.; Bradley, D. D. C. Investigation of amplified spontaneous emission in oriented films of a liquid crystalline conjugated polymer. *Synth. Met.* **2003**, *139*, 727−730.
(48) Grivas, C.; Pollnau, M. Organic solid-state integrated amplifiers and lasers. *Laser Photonics Rev.* **2012**, *6*, 419−462.
(49) Wei, Q.; Li, X.; Liang, C.; Zhang, Z.; Guo, J.; Hong, G.; Xing, G.; Huang, W. Recent Progress in Metal Halide Perovskite Micro- and Nanolasers. *Adv. Opt. Mater.* **2019**, *7*, 1900080.
(50) Bonal, V.; Muñoz-Mármol, R.; Gámez, F. G.; Morales-Vidal, M.; Villalvilla, J. M.; Boj, P. G.; Quintana, J. A.; Gu, Y.; Wu, J.; Casado, J.; Díaz-García, M. A. Solution-processed nanographene distributed feedback lasers. *Nat. Commun.* **2019**, *10*, 3327.

https://doi.org/10.1021/acs.macromol.0c02815
Macromolecules 2021, 54, 4342−4350